

Directivity assessment of MEMS microphones in microphone array applications.

Bert Cox Bart Thoen Vincent Rijmen
Liesbet Van der Perre Lieven De Strycker
KU Leuven
Dept. Elektrotechniek (ESAT), DRAMCO research group
Technology Campus Ghent, Gebroeders De Smetstraat 1,
B-9000 Gent, Belgium
info@dramco.be

Abstract

In this paper, the actual omni-directionality of MEMS-microphones (micro-electro-mechanical system) is studied. Commercially available MEMS-microphones are claimed to be omni-directional but there is no real proof for these statements in the data sheets. In addition, is this statement valid for the whole spectrum in which the microphones operate? And, is there any influence of the PCB material they are mounted on? To answer these questions, a directivity assessment was performed. The microphones were placed in an anechoic chamber in which the microphones could rotate automatically, with an accuracy of 0.1125 degrees. The obtained measurement results are depicted in several polar plots. This process was repeated for several types of MEMS microphones. With these plots, it is possible to do a graphical comparison between the different MEMS-microphones. Apart from individual MEMS-microphones, also a linear array of four microphones is measured. Results show the influence of the nearby PCB-components and give an overview of the overall omni-directionality. In addition to this, we can see influences of the PCB material itself.

The measurement-based assessment was performed at different frequencies to derive spectral information.

In the follow up of this paper, we aim to improve the used Angle-Of-Arrival (AoA) algorithms by exploiting the possible attenuations on certain angles. This paper will also explore how the omni-directive features could be exploited in cryptographic applications.

1 Introduction

Acoustic MEMS sensors are getting more and more integrated in our everyday lives with current applications consisting of hearing aides [1], smart phones, urban sensing for smart cities [2], etc. Further development is focused on the use of these microphones in hands-free teleconference systems, voice-based human-computer interfaces, and various assisted listening applications [3]. Recent research on the use of MEMS technology for audio purposes, studied the acoustical-thermal noise caused by the flow resistance of microphone components [4], membrane adaptations to improve the sensitivity and frequency response [5] and some limited distance and directivity measurements of a microphone array [2].

This measurement campaign was executed in function of the SINS-project (Sound INterfacing through the Swarm). The goal of this project is to localize unknown sound sources in a room, using a wireless sensor network. Every sensor node is equipped with a low-power linear MEMS microphone array containing 4 microphones equally spaced apart, as depicted in Figure 1[6].

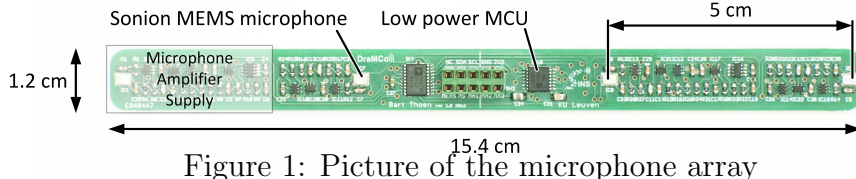


Figure 1: Picture of the microphone array

The used algorithms used on the sensor node assume that the microphones are omni-directional, as stated in the data sheet. This assumption is tested in several conditions: at several frequencies, in different planes, with different PCB thicknesses and this for several commercially available MEMS-microphones. In section 2 of this paper, the measurement set-up is described, followed by an overview of the different measurements in section 3. Section 4 will discuss the obtained results while the last section forms a conclusion on this measurement campaign.

2 Measurement Set-Up

Figure 2 shows the built set-up in the semi-anechoic chamber at the Vrije Universiteit Brussel *. It consists of a speaker placed 1.5 m high facing a microphone (or array) mounted on a 3D-printed structure that is driven by a stepper motor. The two entities are separated by a distance of 2 m and are positioned in the center of the chamber, far enough from the walls. The 3D-printed structure has two functions: the first one is to easily mount the array and microphones and this in several planes. The second one is to create a distance between the base structure, consisting of the stepper motor and the mounting plate, necessary to prevent possible reflections and to shield it from noises induced by the stepper motor. The influence of these stepper motor noises, mostly introduced by the hold current of the motor are minimal and don't affect the measurements. The stepper motor itself has an angular accuracy of 0.1125° and is controlled by a computer outside the semi-anechoic chamber, this to avert possible noise injection.

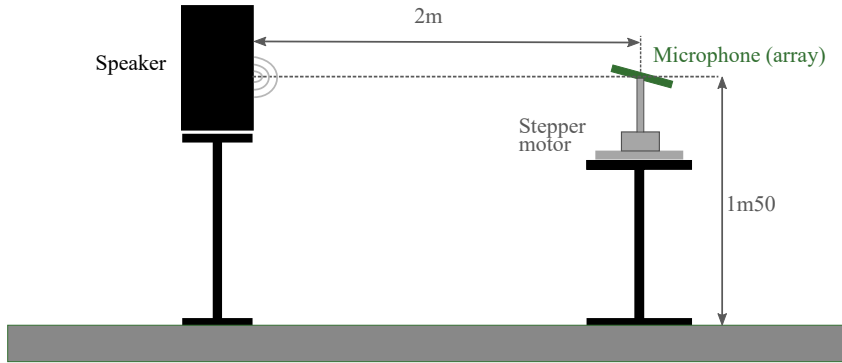


Figure 2: Set-up in semi-anechoic chamber.

The speaker and the four outputs of the array are connected to a sound table via a DI-unit (Differential Input). The received sound signal is amplified by two sources: firstly there is the amplification on the microphone circuit itself using an operational amplifier [6], secondly in the sound table. Both the amplifications are tuned in order to have an equal overall amplification that doesn't drive the received signals into saturation. The speaker and the recording of the responses are managed with Cubase software †. Further processing of the received WAV-files is done with Audacity and Matlab.

*ETRO-VUB Noisey Elephant Studios: http://www.etrovub.be/RESEARCH/Nosey_Elephant_Studios

†Cubase software: <https://www.steinberg.net/en/products/cubase>

3 Measurements and Processing

The measurement campaign can be split up into two parts. The first couple of measurements characterize the speaker, in a way that the final polar plots has as little as possible external influences. The second part of the campaign consists of measuring the bespoke microphone characteristics.

3.1 Speaker Measurements

Table 1 shows the A-weighting values of the speaker at different frequencies, all a multiple octaves higher or lower than the central 1 kHz frequency. The measurements were obtained with a Brüel and Kjaer hand held 2250L dB-meter at the exact position of the microphones. Plotting these values, it can be clearly seen that this speaker follows the typical dB(A) logarithmic curve. A familiar shape can be seen as well in the flat response factors that will be handled in the next subsection.

Table 1: A-weighting values of the speaker

Freq (Hz)	62.5	125	250	500	1000	2000	4000	8000	16000
dB(A)	51.3	60.5	73.9	78.2	84.5	76.4	79.2	79.2	70.7

3.2 Microphone Measurements

The second part of the measurement campaign consists of characterizing several microphone parameters. The basic principle used in every measurement covers the two most crucial parameters: obtaining the frequency response at several incident angles. A single measurement consists of: recording the sequential frequencies played from a single sound file and updating the angle via the stepper motor (in steps of 3° or 6°). These measurements are repeated until the microphone or array made a 360° revolution. Then the following influences on the omnidirectionality are tested:

1. The type of MEMS microphone. Several commercially available MEMS-microphones were tested, from different price-ranges and from different manufacturers. (the Invensense INMP504, the Sonion N8 and the Invensense ICS40310)
2. The distance to the rotation axis. When placed in an array, the microphones don't rotate around their own axis anymore but around the center of the array.
3. The incident plane. This is done by rotating the microphone array around the abscissa and the ordinate to see if it is possible to use the array in several planes for potential 3D-positioning methods.
4. The PCB-material on which the microphone is mounted on. Two thicknesses of the typical FR4 material were tested.

3.3 Processing

The recorded files at the recording panel are WAV-files that represent an amplified voltage. For every microphone at every frequency and at every incident angle the RMS value gets calculated out of these audio files. This is done by averaging the received signal over a period of 3 s. Next the Flat Response Factor (FRF) gets calculated. This factor is needed to filter out the audio profile of the speaker, in this way the adapted RMS-values only represents the “pure” microphone response. Again, for every frequency at an incident angle of 0° an RMS-value (RMS_{flat}) gets calculated, but this

time via of the flat response microphone (Earthworks M30). These flat response RMS-values (FR-RMS) will be used to calculate every FRF-value. The FRF itself can be found with the following equation:

$$FRF @ f_1 = \frac{RMS_{flat} @ f_1}{RMS_{Mic} @ f_1}$$

RMS_{Mic} in this equation represents the RMS-value of the recording at an incident angle of 0° and at the corresponding frequency of RMS_{flat} . To filter out the audio profile of the speaker, every RMS value gets multiplied with the FRF.

$$RMS_{adapt} @ f_x, \alpha_y = \frac{RMS_{flat} @ f_x}{RMS_{Mic} @ f_x, \alpha_y}$$

The polar plots are obtained by searching the maximum, adapted RMS value (RMS_{max}), and normalizing all the RMS-values to RMS_{max} . Figure 3 shows such a polar plot. 0° represents the incident sound wave perpendicular to the microphone. As stated, the radial axis is normalized to the maximum FRF-adapted RMS value. When combined with the values from table 1 , it is possible to plot the absolute dB(A) values.

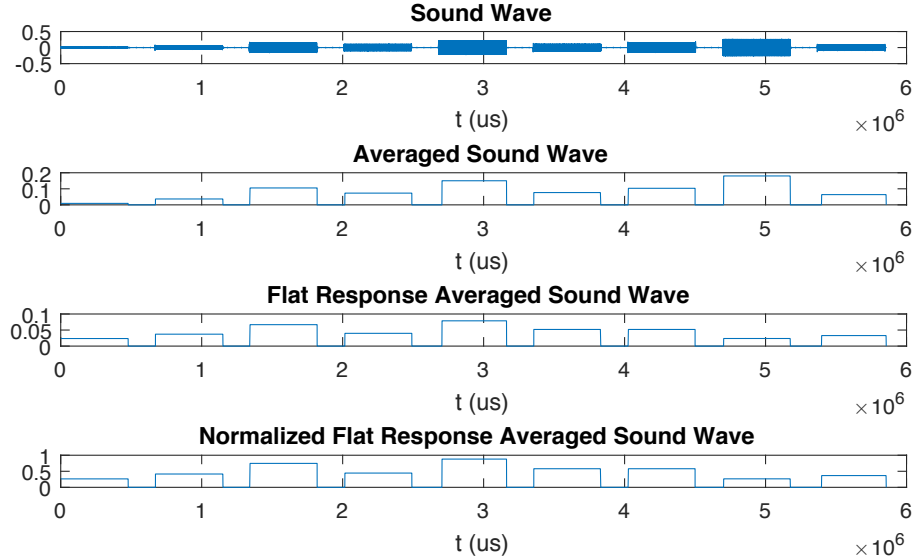


Figure 3: Processing to get the adapted RMS-values out of the WAV-files.

4 Results

4.1 Individual Microphone

Figure 4 shows the omnidirectionality of an individual Sonion N8 MEMS microphone. This microphone is currently used in the current SINS-project arrays and selected for its ultra low power consumption of only $13 \mu\text{A} @ 1 \text{ V}$. The colors on the plot refer to the different frequencies (in Hz) at which the omnidirectionality is measured. It is clear that we can divide this figure into two parts: the left part of figure 5 shows the polar plot for frequencies below 1 kHz, the right part above this frequency. The first figure confirms the proposed condition of omnidirectionality. It shows nearly perfect concentric circles and shows the sensitivity of the microphone at the imposed frequencies.

The latter part, tells a different story: the omnidirectionality diminishes at higher frequencies. This is due to standing waves introduced by the non-anechoic character of the room. The wavelength of these waves approach the size of the microphone's dimensions. Suppose a sine wave with a frequency of 16 kHz and the speed of sound is 343 m/s, than the wavelength in this case is 0.0214 m. The maximum difference in such a sine wave can be found at half a wavelength, meaning even the smallest misalignment of the microphone to the rotation axis introduces a difference in received power. Next subsection will show what happens when the distance between the rotation axis and the microphone increases.

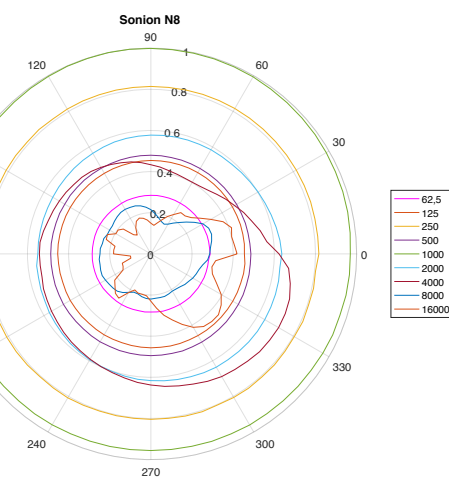
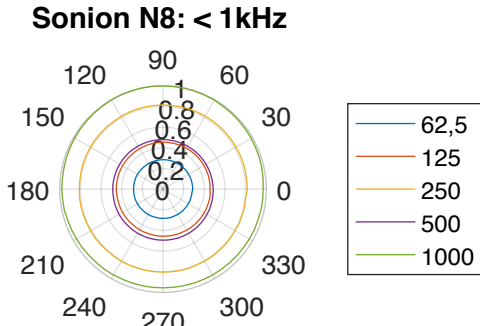


Figure 4: Sonion N8 spectral response.
The microphone increases.

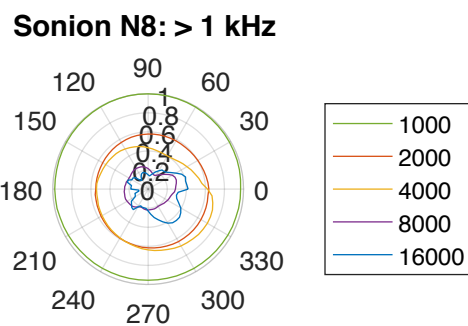


Figure 5: Splitted polar plot of the Sonion N8 microphone.

4.2 Microphone Array

Next to the individual microphone, the array was tested. It is important to note that the backside of the array, where the microphone inlet is positioned, is blank PCB material where no components are placed on. This results in the lack of influence of neighboring components. In figure 6, the omnidirectionality of the 4 microphones on the array are shown at the most sensitive frequency (1 kHz). Out of this, we can distinct 2 microphone pairs: mics 1 and 4, and mics 2 and 3. These microphone pairs have the same distance to the rotation axis, and have similar polar plots rotated over 180°. At a 180° angle difference, each microphone of a pair has the same distance and incident angle as the opposite one.

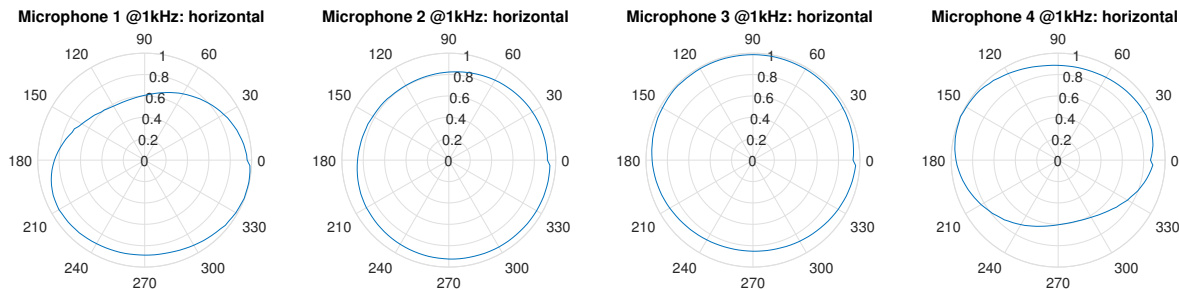


Figure 6: Polar plots of array microphones @ 1 kHz.

Already at this frequency, we can see that a better omnidirectionality is obtained by positioning the microphones closer to the rotation axis of the array. The difference

between the input level at 0° and 180° of the same microphone is due to the orientation of the microphone input. At 0° the inlet of microphone 1 is directly pointing to the speaker, at 180° the inlet is pointing to the other side. Another influence on the sensitivity when comparing the microphone pairs are the deviations on internal microphone components.

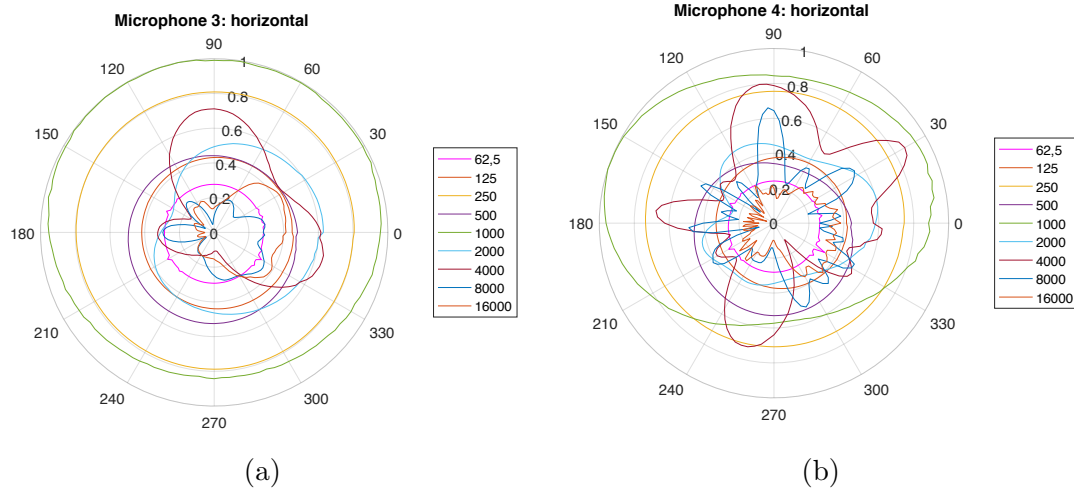


Figure 7: Polar plot of microphone 3 and 4 of the array.

Next, the microphones are compared at different frequencies. To visualize this, microphone 3 and 4 are selected (figure 7). At lower frequencies, the omnidirectionality is still maintained. Yet, this omnidirectional character reduces faster at higher frequencies than in figure 4. The influence of the standing wave increases not only with the frequency, but with the distance to the center of the array: a better omnidirectionality is obtained by positioning the microphones closer to the rotation axis. By increasing this distance, the path the microphone makes when being rotated between two or more angular steps, gets in the range of the wavelengths of the lower frequencies. When taking a closer look at the higher frequencies of microphone 4 (figure 7b) we can see that the response fluctuates more between two consecutive angles in comparison to the figure 7a and 4. In this way, the effect of increasing the offset to the rotation axis is dual: not only is there an alteration introduced at lower frequencies, it increases at higher frequencies. Next to these response fluctuations another effect can be seen at these higher frequencies. The microphone response decreases when the inlet of the MEMS turns away from the sound source.

To test if it is possible to use the array for 3 dimensional purposes, we did the same measurements with the array positioned vertically. This time, the rotation axis runs through the 4 microphones. Figure 8 shows that the influence of the standing wave is minimal, both on the amount of fluctuations as well as the frequency at which the alterations are introduced.

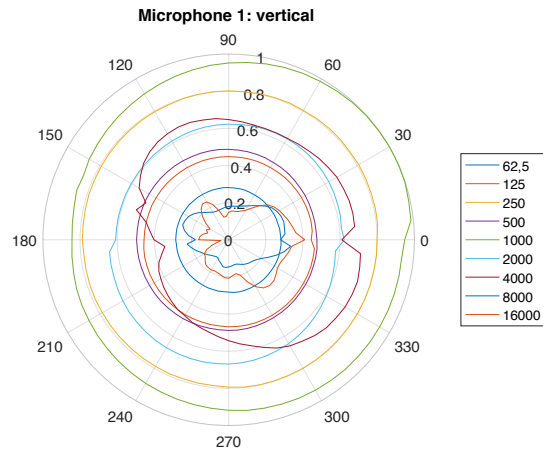


Figure 8: Spectral response of microphone in array when placed vertical.

4.3 Microphone Comparison & PCB material

With the last results we can check if there is a lot of difference between commercially available MEMS microphones. In figure 9 there are 3 types of microphones compared, the Invensense INMP504 (< \$2), the Sonion N8 (< \$8) and the Invensense ICS40310 (< \$3). From the start, it is evident that the low-end INMP504 isn't the best choice when designing an array for precise positioning. Two factors affect the lower sensitivity and the standing wave patters at lower frequencies. This microphone normally uses a larger supply voltage rating (3.4 V) compared to the other two (1.9 V), this has negative effects on the output levels. The other factor is the narrower sound inlet at the PCB material.

When we compare the N8 (higher-end) and the ICS40310 (mid-range), it is harder to find distinctive elements, as they both have the same spectral response. Only the response at the highest frequency and the sensitivity between these two is different, with ICS40310 being the most sensitive.

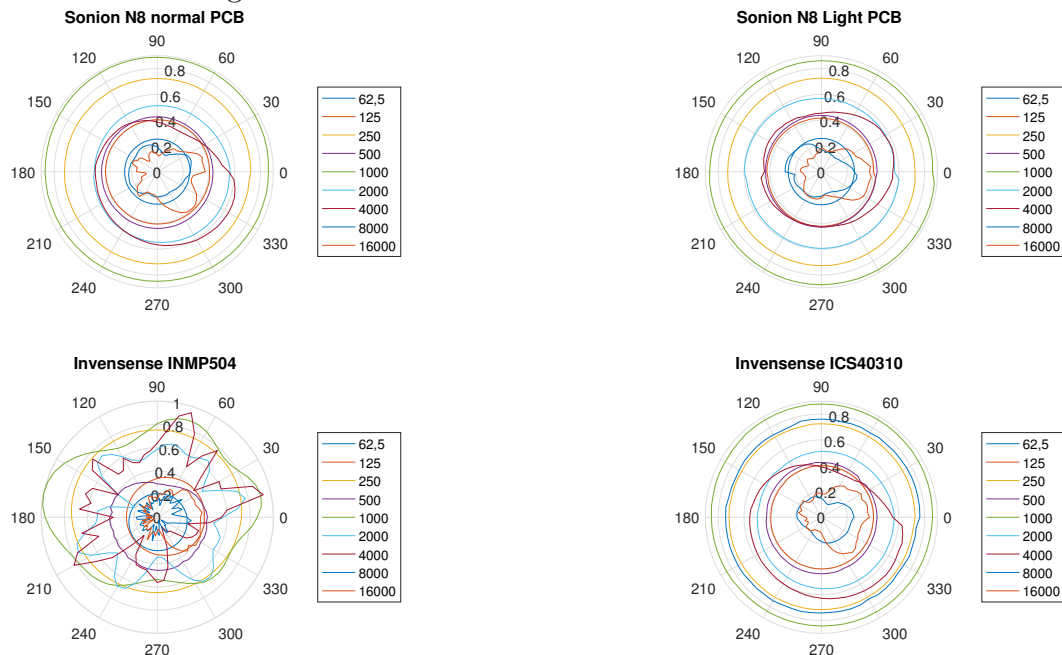


Figure 9: Comparison of different microphones.

Next to these three polar plots in figure 9, there is a fourth one: the frequency response of the Sonion N8 mounted on a thinner (0.25 mm) FR4-based PCB-material. The lower response can be explained through the Helmholtz resonance. Components between the external environment and the membrane acts as a wave guide that shape the frequency response REF. Figure 10[‡] shows the cross section of a MEMS microphone. The narrow sound inlet, in combination with the front and back chamber creates a Helmholtz-resonator. The same principle is used to make sound when blowing on top of an empty bottle. The Helmholtz resonance frequency is given by:

$$f_h = \frac{c}{2\pi} \sqrt{\frac{A_H}{V_C L_H}}$$

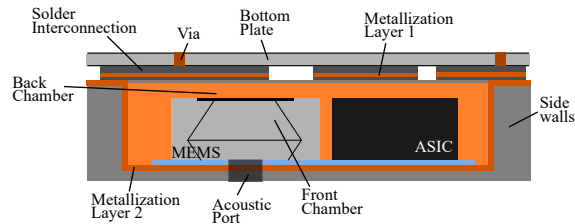


Figure 10: Cross section of microphone assembly.

[‡]Based on figure of 2013 MEMS Journal by STMicroelectronics

With c being the speed of sound, A_H the sound-inlet area, V_C the volume of the cavity formed by the front and back chamber and L_H is the length of the inlet.[7] Decreasing the inlet length will increase the resonant frequency and causes the sensitivity to lower at higher frequencies. This lower response is clearly visual on the radial axis of the “Sonion N8: light PCB” polar plot.

5 Conclusion

The omnidirectionality, as stated in the datasheets of the microphones, really comes forward when we look at the frequency responses in the different situations. At higher frequencies we can state that there is an influence of the standing waves, introduced by the speaker and semi-anechoic room. These can affect the results when used in Angle-Of-Arrival measurements. Filtering the sound signal, via a low pass filter with a cut off frequency at 4 kHz, can have a positive effect. Another solution would be attenuating signals coming from certain angles. However, it needs to be stated that in real world applications no such pure sine-waves will ever take place. Out of this, in combination with the limited range of the speak spectrum (<4 kHz), we can conclude that the overall omnidirectionality will be maintained. The distance to the rotation axis, the inlet area size and PCB-thickness are the factors that have a large effect on the sensitivity. Out of the comparison between the different microphones we can conclude that the mid range ICS40310 is the best choice for future applications.

Future work comprise testing these microphones in a complete anechoic chamber to check if there is still an influence of the standing waves. In this environment, ultrasonic microphones could be tested as well for future positioning projects that are undetectable for humans. Other research could explore how favorable these omni-directive results could be exploited in cryptographic applications.

References

- [1] K. WH, R. Zhang, P. Huang, J. Guo, X. Ye, D. Young, and C. Megerian, “Studies of mems acoustic sensors as implantable microphones for totally implantable hearing-aid systems.” *137th AES Convention*, 2014.
- [2] C. Mydlarz, S. Nacach, E. Rosenthal, M. Temple, T. H. Park, and A. Roginska, “The implementation of mems microphones for urban sound sensing,” *IEEE Trans Biomed Circuits Syst.*, vol. 3, no. 5, pp. 277–285, 2009.
- [3] K. Kowalczyk, S. Wozniak, T. Chyrowicz, and R. Rumian, “Embedded system for acquisition and enhancement of audio signalsr,” *Signal Processing - Algorithms, Architectures, Arrangements, and Applications Conference Proceedings*, pp. 68–71, 2016.
- [4] B. Kim and H. Lee, “Mems microphone with a micro helmholtz resonator,” *Sensors Journal*, vol. 15, no. 12, pp. 6853–6860, 2015.
- [5] C. H. Je, J. Lee, W. S. Yang, and J. Kim, “The Novel Sensitivity Improved Surface Micromachined MEMS Microphone with the Center-Hole Membrane,” in *2011 Procedia Engineering*, 2011, pp. 583–586.
- [6] G. Ottoy, B. Thoen, and L. D. Strycker, “A low-power MEMS microphone array for wireless acoustic sensors,” in *2016 IEEE Sensors Applications Symposium (SAS)*, April 2016, pp. 1–6.
- [7] H. Takahashi, A. Suzuki, E. Iwase, K. Matsumoto, and I. Shimoyama, “Acoustical-thermal noise in a capacitive mems microphone,” *Journal of Micromechanics and Microengineering*, vol. 22, no. 8, p. 085019, 2012.